

Lattice dynamics and vibrational specific heat of MgO microcrystals*

T. S. Chen, F. W. de Wette, Leonard Kleinman, and D. G. Dempsey

Department of Physics, University of Texas, Austin, Texas 78712

(Received 3 June 1977)

In this paper we treat the lattice dynamics of microcrystals (clusters) of MgO in the context of the Kellermann rigid-ion model. Clusters of 180 and 900 ions are studied, both unrelaxed and relaxed. Extensive use of the cluster symmetry (space group D_{2h}) allows us to solve the dynamical problem of the large cluster. The effects of size and of relaxation on the dynamics and the vibrational specific heat are evaluated. It is found that size effects are simple, that is, proportional to cluster size and ratio of surface to bulk ions. On the other hand, relaxation effects are very significant in that unrelaxed clusters do not satisfy the condition of rotational invariance; this leads to the wrong behavior of the cluster-excess heat capacity over the entire temperature range.

I. INTRODUCTION

In recent years a fair amount of experimental and theoretical interest has been devoted to a variety of properties of ionic microcrystals, such as infrared absorption, Raman scattering, and heat capacity. The theoretical description of each of these phenomena requires a treatment of the vibrational modes of microcrystals. Such treatments have been given both in the context of continuum theory^{1,2(a)} as well as with lattice dynamics.^{2(b)} The latter approach becomes necessary when the lattice properties are important, as is the case when the crystallite size is small compared to the wavelength of the absorbed or scattered light, or for the description of thermodynamic properties at sufficiently low temperatures. Despite the fact that a lattice-dynamical calculation becomes unpractical for crystallites of more than a thousand ions, such an approach allows the study of the influence of size variation on the optical and thermodynamical properties of small crystallites in a reasonably realistic fashion.

Several years ago, Genzel and Martin^{2(b)} carried out a lattice-dynamical calculation for MgO microcrystals (of up to 180 ions) to evaluate the influence of surface and size effects on the dynamical and infrared properties of such systems; in this work the relaxation of the microcrystals was not taken into account. However, in recent work on slab-shaped crystals, Chen and de Wette³ have demonstrated that surface relaxation can have extremely important effects on surface vibrational spectra. This strongly suggests that relaxation cannot be neglected in the study of the dynamical properties of microcrystals with a high surface-to-volume ratio.

In the present paper we study the dynamics of small microcrystals (clusters) of MgO containing 180 and 900 ions, with and without relaxation. This

enables us to study the effects of increase in size (by a factor of 5) and of relaxation on the dynamics of these clusters. Since Chen *et al.*⁴ have recently made a detailed study of the surface thermodynamic properties of ionic crystal slabs (including MgO), it seemed worthwhile, for comparison with the slab results, to evaluate the cluster-excess heat capacity of these MgO microcrystals.

From the experimental point of view, measurements of the heat capacity of small particles (powders) form the most direct approach to the vibrational contributions to the surface thermodynamic functions. Unfortunately, however, despite a growing interest in surface thermodynamics, very few direct measurements of the heat capacity of powders have been made up to the present. A similar situation exists with respect to theoretical work; despite the fact that there have been a number of analytical treatments of surface thermodynamic properties, very few calculations of these properties were based on sufficiently realistic crystal models to allow a detailed comparison with experimental measurements such as exist. For a more complete discussion of these matters we refer to Ref. 4. We hope that the present work will help to stimulate further experimental and theoretical interest in this area.

II. CALCULATION

Following Ref. 2(b) we have used the Kellermann rigid-ion model (KRIM) for the ionic interactions in the cluster. Although the KRIM is known to be deficient in that it neglects polarization, it enables us to calculate the cluster relaxation in a reasonably simple fashion [which the shell model (SM), used in earlier calculations⁵ on MgO slabs, does not]. Moreover, as Chen *et al.*^{4,6} have shown in earlier work on NaCl slabs, the low-temperature specific-heat results obtained with the KRIM and

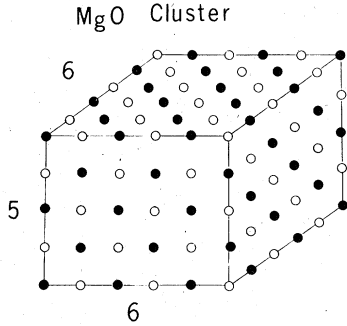


FIG. 1. Small cluster of MgO (180 ions) with D_{2h} symmetry. The large cluster (900 ions) has the same symmetry.

the SM are in quite good agreement, despite differences in the details of the dynamics. This seems to result from the fact that the specific heat is mainly determined by the long-wavelength acoustic modes, whereas the differences between the KRIM and the SM are primarily evident in the optical modes.

In the present work we have not taken into account anharmonic effects and thermal expansion since they would substantially complicate the calculations. Although these phenomena should certainly be included in a full description of the dynamics and thermodynamics of small crystallites, it is reasonable to assume that at the low temperatures of interest here they play only a minor role.

The calculations have been carried out for rectangular clusters bounded by (001) surfaces. The reason for choosing clusters of this symmetry are the following: First, the earlier calculations of Genzel and Martin,^{2(b),9} with which we want to compare our results, were carried out for clusters of this symmetry, but more importantly, it appears from electron micrographs of the MgO smoke used in Rieder and Hörl's^{10,11} experiments that this smoke indeed consisted of microcrystals of this symmetry. On the basis of equilibrium energy considerations one might have expected the crystallites to have close to spherical shape, but this appears not to be the case. Apparently, the formation of the smoke is not a process in which complete equilibrium is reached.

We have chosen rectangular clusters of $6 \times 6 \times 5 = 180$ ions (see Fig. 1) and $10 \times 10 \times 9 = 900$ ions (called "small" and "large" in what follows). This particular shape cluster was chosen because it has D_{2h} symmetry (with [001], and [110] and [110] as the twofold rotation axes); this has no degenerate irreducible representations which is desirable because a maximum number of independent vibrational frequencies are required for obtaining reasonable density-of-states functions. At the

same time the number of irreducible representations is large (eight) so that our 2700×2700 dynamical matrix could be block diagonalized into eight matrices, the largest of which was 370×370 .

A. Relaxation procedure

The calculations were carried out for unrelaxed and relaxed clusters. In an unrelaxed cluster the ions occupy the same positions as they do in the bulk, but these are not the positions of static equilibrium because of the finite size of the cluster. To obtain the relaxed positions we use the fact that in static equilibrium the static potential energy of the cluster is minimum so that the forces on the ions are zero.

The expansion of the potential energy Φ of the crystal, in terms of the particle displacements $u_\alpha(l\kappa)$, has the form

$$\Phi - \Phi_0 = \sum_{l\kappa\alpha} \Phi_\alpha(l\kappa) u_\alpha(l\kappa) + \frac{1}{2} \sum_{\substack{l\kappa\alpha \\ l'\kappa'\beta}} \Phi_{\alpha\beta}(l\kappa; l'\kappa') u_\alpha(l\kappa) u_\beta(l'\kappa') + \dots, \quad (1)$$

where Φ_0 is the potential energy of the configuration about which the expansion is made, $u_\alpha(l\kappa)$ is the α component (x, y, z) of the displacement of the ion of the kind κ , at the site l , and

$$\Phi_\alpha(l\kappa) = \left. \frac{\partial \Phi}{\partial u_\alpha(l\kappa)} \right|_0, \quad (2a)$$

$$\Phi_{\alpha\beta}(l\kappa; l'\kappa') = \left. \frac{\partial^2 \Phi}{\partial u_\alpha(l\kappa) \partial u_\beta(l'\kappa')} \right|_0. \quad (2b)$$

$\Phi_\alpha(l\kappa)$ is the negative of the α component of the force acting on the ion ($l\kappa$). In the KRIM these forces contain contributions from the long-range point-charge interaction, and from the short-range repulsive pair interaction which is described by the Born-Mayer potential

$$\Phi^s = \lambda e^{-r_{ij}/\rho}. \quad (3)$$

Here r_{ij} is the nearest-neighbor distance, and $\lambda = 3.585 \times 10^{-9}$ erg and $\rho = 2.538 \times 10^{-9}$ cm are the Born-Mayer constants for the nearest-neighbor Mg-O interactions. These parameters, as well as the effective ionic charge $e^* = 1.52e$ (e is the electron charge) for the Coulomb interactions are the ones used in Ref. 2(b) and were derived by Kellermann's method⁷ from the condition of bulk lattice stability and two relations involving the reststrahl frequency and the compressibility.

A reasonably fast procedure to find the relaxed equilibrium configuration of the cluster is the following. Starting from the bulk configuration, for which the forces $-\Phi_\alpha(l\kappa)$ are not zero, we move the

ions over small distances, proportional to the forces on them. That is, we give the ions displacements of the form

$$u_{\alpha}(l\kappa) = -v\Phi_{\alpha}(l\kappa). \quad (4)$$

Substituting these displacements into Eq. (1) we find,

$$\begin{aligned} \Phi - \Phi_0 = & -v \sum_{l\kappa\alpha} \Phi_{\alpha}^2(l\kappa) \\ & + \frac{1}{2}v^2 \sum_{\substack{l\kappa\alpha \\ l'\kappa'\beta}} \Phi_{\alpha\beta}(l\kappa; l'\kappa') \Phi_{\alpha}(l\kappa) \Phi_{\beta}(l'\kappa'). \end{aligned} \quad (5)$$

If v is chosen sufficiently small, $\Phi - \Phi_0$ will be negative, and the new configuration, resulting from the displacements (4), is closer to the ultimate equilibrium configuration. This leads to an iteration procedure which is continued by calculating the new $\Phi_{\alpha}(l\kappa)$ and $\Phi_{\alpha\beta}(l\kappa; l'\kappa')$ and repeating the whole procedure. If in each step of this iteration procedure $\Phi - \Phi_0$ continues to be negative and $|\Phi - \Phi_0|$ and $|\Phi_{\alpha}(l\kappa)|$ continue to decrease, we know that we are approaching the equilibrium configuration.

A suitable value for v follows from Eq. (5), which is quadratic in v and goes through the origin (i.e., $\Phi - \Phi_0 = 0$ for $v = 0$). Starting from a nonequilibrium configuration, $\Phi - \Phi_0$ is negative for small positive v , but becomes positive for large v . Hence $\Phi - \Phi_0$ has a minimum for some small $v = v_{\text{optimum}}$ given by

$$v_{\text{opt}} = \frac{\sum_{l\kappa\alpha} \Phi_{\alpha}^2(l\kappa)}{\sum_{\substack{l\kappa\alpha \\ l'\kappa'\beta}} \Phi_{\alpha\beta}(l\kappa; l'\kappa') \Phi_{\alpha}(l\kappa) \Phi_{\beta}(l'\kappa')} \quad (6)$$

Choosing $v \lesssim v_{\text{opt}}$ we know that in carrying out the displacements (4) we are moving closer to the equilibrium configuration. Unfortunately, this method for choosing v is computationally time consuming because for each new configuration, v_{opt} has to be reevaluated. In practice it turned out that this method works fine for the relaxation of the small cluster, but that it is far too time consuming for the relaxation of the large cluster. In the latter case, therefore, we have assumed values for v , guided by our experience with the small cluster. The approach to the equilibrium configuration is monitored by calculating the first derivative term $\sum \Phi_{\alpha}^2(l\kappa)$ which should diminish after each step of the iteration. This procedure avoids calculating the denominator of Eq. (6).

In the case of the small cluster, where v was computed, 33 steps in the iteration reduced the largest force component in the cluster by a factor of 6.5×10^{-3} . On the other hand, during the first 15 of these steps $\Phi - \Phi_0$ was reduced by a factor of

10^{-4} . Hence it is clear that $\Phi - \Phi_0$ gives a more optimistic picture of the approach to equilibrium than do the forces $-\Phi_{\alpha}(l\kappa)$. Since the calculation of $\Phi - \Phi_0$ requires more computational effort than $\Phi_{\alpha}(l\kappa)$, in practice we have judged the approach to the equilibrium configuration by monitoring the decrease in the forces alone.

In the iteration procedure for the large cluster, where we used estimated values for v , a total of 120 steps in the iteration procedure reduced the largest force component by a factor 4×10^{-3} . The probable reason for needing many more iteration steps to obtain about the same force reduction as for the small cluster is that the estimated values of v were not optimum. In particular, if at any stage of the calculation an iteration had a larger value of $\sum_{l\kappa\alpha} \Phi_{\alpha}^2$ than the preceding iteration, we discarded that iteration and reduced the magnitude of v .

In both the small and the large cluster the ions relax inwards such that the cluster becomes slightly rounded: The corner ions and their neighbors are relaxed most, the edge ions second most, and the surface ions least, especially those in the middle of the face.

Some time ago Anderson and Scholz⁸ evaluated relaxation effects in ionic microcrystals (including MgO) by minimizing the static energy with respect to the positions of only the surface ions, and the lattice constant of the remainder of the crystal. Despite this restriction, their results for clusters of up to 20 ions are in qualitative agreement with our results for very small clusters (not reported here). The strength of the present method is that the forces on the ions are used as a guide in changing the ionic positions, so that all ions can be included in the minimization procedure. This latter fact is of basic importance. It can be shown that the condition of rotational invariance is only satisfied for a crystal which is in its configuration of lowest potential energy. This is borne out by our calculations; the lattice-dynamical solution of the unrelaxed cluster yielded three nonzero rotational frequencies. After relaxation these frequencies were reduced in value, but not as much as one would naively expect; apparently the vanishing of the rotational frequencies is by far the most sensitive test of approach to the equilibrium configuration.

B. Solution of the dynamical equations

In the harmonic approximation the equation of motion of the ion ($l\kappa$) is

$$M_{\kappa} \ddot{u}_{\alpha}(l\kappa) = - \sum_{l'\kappa'\beta} \Phi_{\alpha\beta}(l\kappa; l'\kappa') u_{\beta}(l'\kappa'). \quad (7)$$

It is customary to assume an oscillatory solution

for Eq. (7), that is,

$$u_{\alpha}(l\kappa) = \frac{\xi_{\alpha}(l\kappa)}{M_{\kappa}^{1/2}} e^{-i\omega t}. \quad (8)$$

Substituting Eq. (8) into Eq. (7) we obtain the eigenvalue equation

$$\omega^2 \xi_{\alpha}(l\kappa) = \sum_{l'\kappa'\beta} D_{\alpha\beta}(l\kappa; l'\kappa') \xi_{\beta}(l'\kappa'). \quad (9)$$

$D_{\alpha\beta}$ is the matrix element of the dynamical matrix which can be expressed in terms of Coulomb and short-range interactions

$$D_{\alpha\beta}(l\kappa; l'\kappa') = \frac{1}{(M_{\kappa} M_{\kappa'})^{1/2}} [\Phi_{\alpha\beta}^c(l\kappa; l'\kappa') + \Phi_{\alpha\beta}^s(l\kappa; l'\kappa')], \quad (10)$$

with

$$\Phi_{\alpha\beta}^c(l\kappa; l'\kappa') = e_{\kappa}^* e_{\kappa'}^* \left(\frac{\delta_{\alpha\beta}}{|r(l\kappa; l'\kappa')|^3} - \frac{3r_{\alpha}(l\kappa; l'\kappa')r_{\beta}(l\kappa; l'\kappa')}{|r(l\kappa; l'\kappa')|^5} \right) \quad (11)$$

and

$$\Phi_{\alpha\beta}^s(l\kappa; l'\kappa') = - \left(\frac{e^2}{4r_0^3} \right) \times \left((A - B) \frac{r_{\alpha}(l\kappa; l'\kappa')r_{\beta}(l\kappa; l'\kappa')}{|r(l\kappa; l'\kappa')|^2} + B\delta_{\alpha\beta} \right). \quad (12)$$

Here, A and B are short-range parameters depend-

ing on the interparticle distance r ; they are related to the Born-Mayer parameters λ and ρ by the following relations:

$$A(r) = \left(\frac{4r_0^3}{e^2} \right) \frac{d^2\Phi^s}{dr^2} = \left(\frac{4r_0^3}{e^2} \right) \frac{\lambda}{\rho} e^{-r/\rho}, \quad (13)$$

$$B(r) = \left(\frac{4r_0^3}{e^2} \right) \frac{1}{r} \frac{d\Phi^s}{dr} = - \left(\frac{4r_0^3}{e^2} \right) \frac{\lambda}{\rho r} e^{-r/\rho}. \quad (14)$$

III. RESULTS AND DISCUSSION

A. Cluster-excess phonon density of states

In Fig. 2 we present the phonon density-of-states functions for the unrelaxed and relaxed small cluster. The main differences are that the spectrum for the relaxed cluster extends to slightly higher frequencies than that of the unrelaxed cluster, because the small inward relaxation gives rise to slightly stiffer forces; in addition the main central peak is broader. This will turn out to have important consequences for the cluster-excess density of states and consequently for the cluster-excess specific heat.

The small broad peak near zero in the unrelaxed case represents the three zero translational frequencies, and the three nonzero (but small) rotational frequencies. In the relaxed case, the sharp peak at zero represents the three zero translational frequencies, and the three rotational frequencies which have been substantially reduced by the relaxation of the cluster. Specifically, the relaxa-

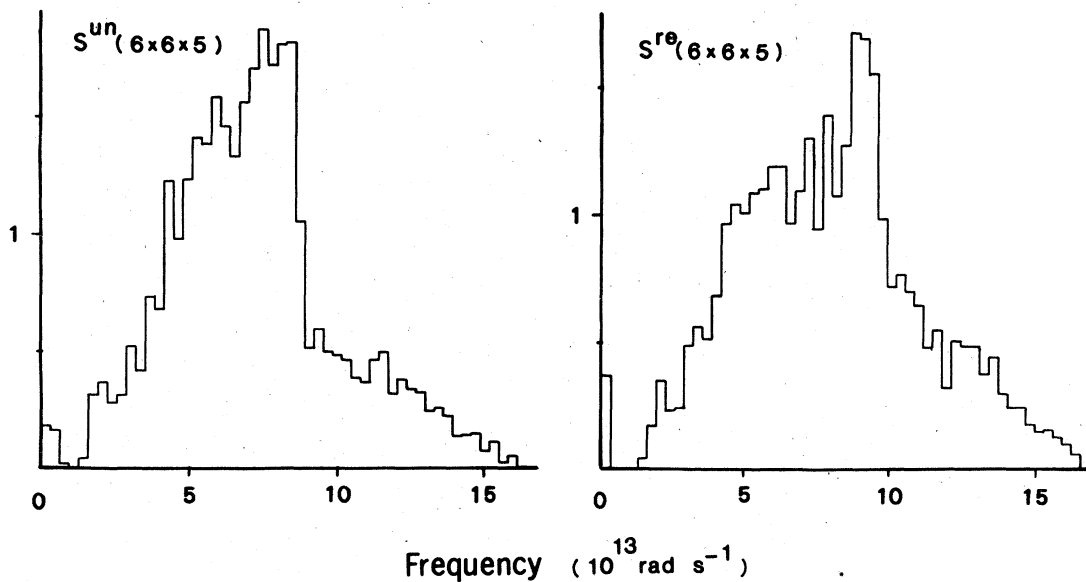


FIG. 2. Phonon density-of-states histograms for the unrelaxed and relaxed small clusters of MgO (S^{un} and S^{re} , respectively). The vertical scale is such that the total area under the curve is normalized to one.

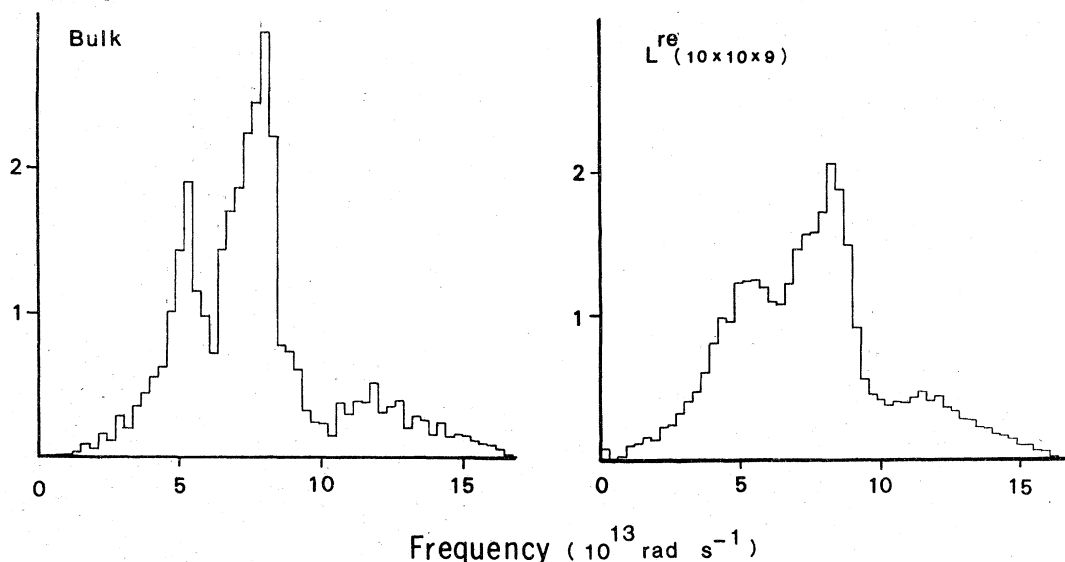


FIG. 3. Phonon density-of-states histograms for the bulk and the relaxed large cluster of MgO. Vertical scale as in Fig. 2.

tion causes a reduction in one of the rotational frequencies by a factor of 4 from 4.7×10^{12} rad s $^{-1}$ to 1.06×10^{12} rad s $^{-1}$, while the other two are reduced by a factor of 7 from 4.94×10^{12} rad s $^{-1}$ to 7.38×10^{11} rad s $^{-1}$.

It should finally be mentioned that the density of states of the small unrelaxed cluster closely resembles the result of Genzel and Martin,^{2(b)} as it should, because we used the same KRIM in the calculation.

In Fig. 3 we show the bulk phonon density of states of MgO and the density of states of the relaxed large cluster; the bulk results are in good agreement with those of Ref. 2(b). In overall features the relaxed-large-cluster curve is in good agreement with that of the relaxed small cluster (cf. Fig. 2), but much smoother because it contains five times as many frequencies.

The differences between the unrelaxed and relaxed cases are brought out more clearly in the cluster-excess density-of-states function $f^c(\omega)$, which is defined as

$$f^c(\omega) = [f^{\text{cluster}}(\omega) - f^{\text{bulk}}(\omega)], \quad (15)$$

where f^{cluster} and f^{bulk} are the computed spectral densities of the cluster and the bulk, respectively, each normalized to unity (i.e., $\int_0^\infty f(\omega) d\omega = 1$). The functions f^c are presented in Fig. 4: S^{un} for the unrelaxed small cluster, S^{re} for the relaxed small cluster, and L^{re} for the relaxed large cluster. Physically speaking, each of the peaks in f^c contains contributions from surface-, edge- and corner modes (cf. Ref. 9), but we have not disen-

tangled these different contributions here. Comparing the curves for the unrelaxed and relaxed small cluster, it is evident that there are important differences between the locations and the relative strengths of the peaks and valleys: S^{un} has stronger low-frequency peaks, whereas in S^{re} the high-frequency peak is much more pronounced. On the other hand, the spectra for the relaxed cases S^{re} and L^{re} are very similar. The peak and valley locations are the same, but the features of L^{re} are more pronounced because this spectrum is based of five times as many frequencies. The dotted curve with L^{re} is the experimental spectrum, obtained by Rieder and Hörl^{10,11} from neutron scattering experiments on MgO powder. We note that in the lower half of the spectrum the agreement between calculation and experiment is reasonably good, but the very strong high-frequency peak in the calculation has only a weak experimental counterpart, while the broad high-frequency experimental peak has, at best, a very weak computed counterpart. These discrepancies between calculated and experimental results were first noted by Chen *et al.*⁵ in their SM calculations of unrelaxed MgO slabs. Although there are differences between the SM slab results and the KRIM cluster results, neither of these cases gives an explanation for the broad high-frequency peak in the experimental results. Recently, Rieder¹² has speculated that this peak might be due to neutron scattering from a low concentration of hydroxyl ions adsorbed on the surface (cf. Ref. 13). Additional work will be required to resolve these discrepancies.

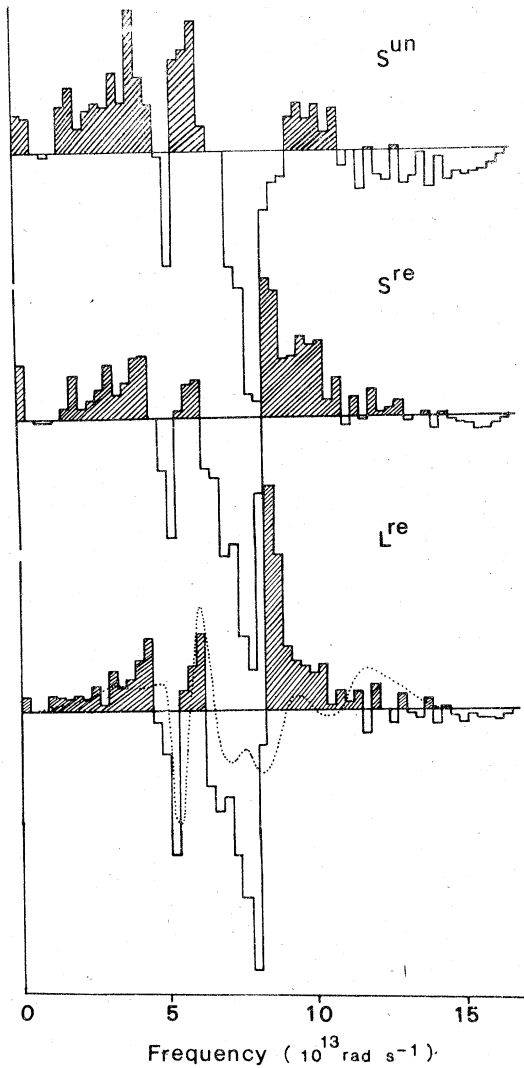


FIG. 4. Cluster-excess phonon density-of-states histograms for the unrelaxed small cluster (S^{un}), and the relaxed small and large clusters (S^{re} and L^{re} , respectively). The vertical scale is arbitrary but the same in the three cases. The dotted curve with L^{re} is determined from neutron scattering experiments (Refs. 10 and 11) and has a different arbitrary vertical scale.

B. Cluster-excess specific heat

The vibrational heat capacity of a system with vibrational frequencies ω_i is given by

$$C_v = k_B \sum_i x_i^2 e^{x_i} (e^{x_i} - 1)^{-2}, \quad (16)$$

where

$$x_i = \hbar\omega_i / k_B T. \quad (17)$$

The cluster-excess specific heat (heat capacity per particle) is defined as

$$c_v^c = N_c^{-1} C_v^c - N_B^{-1} C_v^B, \quad (18)$$

where C_v^c and C_v^B are the heat capacities of cluster and bulk, respectively, and N_c is the number of ions in the cluster and N_B the number of ions in the bulk sample for which C_v^B was calculated.

In Fig. 5 we show the results for c_v^c for the small clusters: S^{un} for the unrelaxed, and S^{re} for the relaxed cluster. The difference between these cases is striking; S^{re} has a peak at 80 °K of height $13.4 \times 10^{-18} \text{ erg}(\text{°K ion})^{-1}$ and at room temperature it has dropped down to 10% of its peak value. On the other hand, S^{un} has a peak at 130 °K of height $27.8 \times 10^{-18} \text{ erg}(\text{°K ion})^{-1}$ and at room temperature is still 60% of its peak value. These differences are a direct result of the differences at low frequencies, between the cluster-excess density-of-states functions $f^c(\omega)$ for these two cases. In particular, the large values of S^{un} are mainly due to the presence of the strong low-frequency peak in $f^c(\omega)$ and the three nonzero rotational frequencies. Finally, the nonzero values of c_v^c at 0 °K result from the inclusion of the three translational and three rotational frequencies in the calculation of c_v^c [Eq. (18)]; the nonzero rotational frequencies of S^{un} account for the smaller 0 °K contribution in S^{un} .

Despite the growing interest in surface thermo-

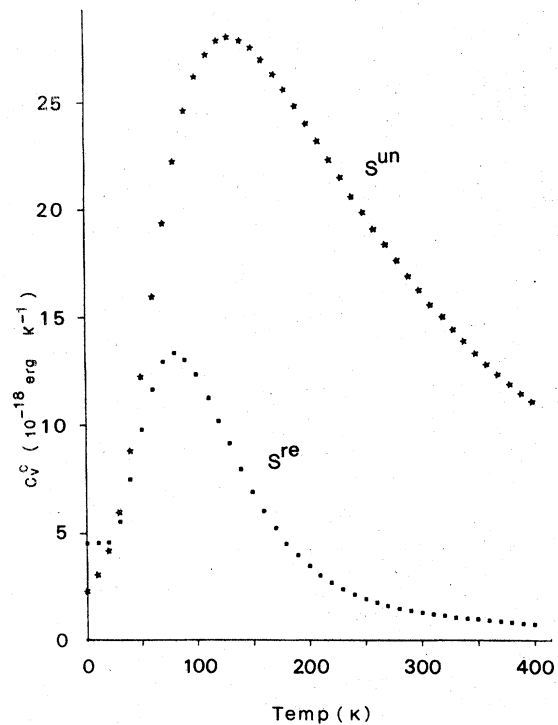


FIG. 5. Surface-excess specific heat per ion c_v^c for the unrelaxed and relaxed small clusters (S^{un} and S^{re} , respectively) as functions of temperature.

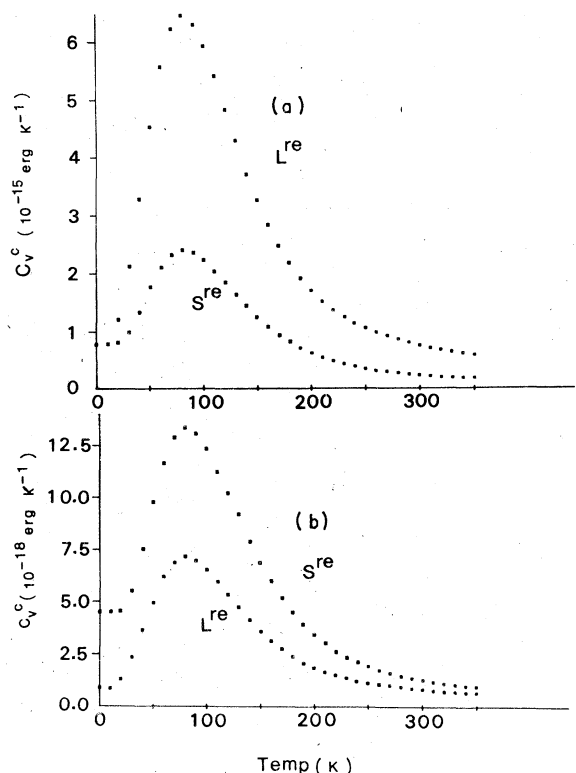


FIG. 6. (a) Surface-excess heat capacities C_v^c of the relaxed small and large clusters (S^{re} and L^{re} , respectively) as functions of temperature. (b) Surface-excess specific heat per ion c_v^c of the relaxed small and large clusters as functions of temperature.

dynamic properties, there are hardly any experimental data with which these calculated results can be compared. Forty years ago, Giauque and Archibald⁴ measured the heat capacity of small MgO particles between 15 °K and room temperature. In 1959, Barron *et al.*¹⁵ combined their own bulk measurements with those of Ref. 14 to obtain the surface-excess heat capacity of MgO. These results indeed show a surface enhancement, but the experimental uncertainties in the data are too large to make a meaningful comparison with our calculated results. For a more extensive discussion of the differences between experimental and theoretical results we refer to Ref. 4.

In Fig. 6 we show a comparison of the cluster-excess specific heat for the relaxed small and large clusters, both as total quantity [Fig. 6(a)] and as quantity per ion [Fig. 6(b)]. For both clusters the peak occurs at the same temperature (80 °K) and the approach to zero for large T is very similar. Since the large cluster contains more surface ions, the total quantity $C_v^c(L^{re})$ is larger [Fig. 6(a)], but since the translational and rotational frequencies

are the same for S^{re} and L^{re} , $C_v^c(L^{re})$ and $C_v^c(S^{re})$ approach the same value for $T \rightarrow 0$ °K. On the other hand, $c_v^c(L^{re})$ [Fig. 6(b)] is smaller than $c_v^c(S^{re})$, because L^{re} has relatively fewer surface ions than S^{re} ; consequently, the 0 °K value of $c_v^c(L^{re})$ is smaller than that of $c_v^c(S^{re})$. This is a size effect that disappears rapidly with increasing cluster size and that will not show up in measurements on real powders because of the larger grain size.

Finally, there remains the question to what extent the present KRIM result for the small unrelaxed cluster (specific surface area 1406 m²/g) can be compared with the SM result for the unrelaxed slab (specific surface area 177 m²/g) of Ref. 4. Points of comparison are the peak maxima of C_v^c and C_v^s , the temperatures T_{max} at which these occur and the decline of C_v^c and C_v^s for increasing temperatures. C_v^c (cf. S^{un} in Fig. 5) has the maximum value of 8.72×10^{-2} erg K^{-1} cm⁻² (expressed in the units of Ref. 4) at $T_{max} = 130$ °K. C_v^s of the slab (cf. Ref. 4, Fig. 3) has the maximum value of 5.98×10^{-2} erg K^{-1} cm⁻² also at $T_{max} = 130$ °. The complete agreement in T_{max} for these two peaks is striking, considering the important differences between these two calculations. Moreover, the high-temperature decline of both peaks is very similar: At 300 °K C_v^c has declined to 58% of its maximum value, while C_v^s of Ref. 4 has declined to 50%. These points of agreement seem to be more than fortuitous. On the other hand, the ratio of the peak heights is only 1.46 instead of 7.94 as one would obtain if C_v^c and C_v^s were strictly proportional to specific surface area, all other things being equal. Whereas an agreement about peak location and shape in the specific heat depends on general similarities between $f^c(\omega)$ and $f^s(\omega)$, a detailed numerical agreement between C_v^c and C_v^s depends on a numerical agreement between $f^c(\omega)$ and $f^s(\omega)$. The latter cannot really be expected because these functions are small differences between cluster and bulk densities of state [Eq. (15)] in the cluster case, and between slab and bulk densities of state in the slab case. In as much as different bulk calculations are involved—KRIM for the cluster, SM for the slab—close agreement cannot be expected. In conclusion then, we can say that the agreement between the unrelaxed cluster and slab cases is extremely gratifying, given the differences between the two calculations.

IV. SUMMARY

In this paper we treated the lattice dynamics and the specific heat of 180-ion and 900-ion clusters of MgO in the context of the Kellermann rigid-ion model. An efficient method was used to obtain the static equilibrium configurations of these clusters (relaxation). We were thus able to evaluate both

size and relaxation effects on the dynamics and the specific heat of these clusters.

The results for the cluster-excess density-of-states functions and the cluster-excess specific heat enable us to judge the relative importance of effects due to size and due to relaxation. The effects of relaxation are intrinsic and pronounced, both in the excess density-of-states functions and in the excess specific heat, and are in evidence over the entire frequency range of $f^c(\omega)$ and over the entire temperature range of C_v^c . It turns out, however, that size effects are simply proportional to the number of ions involved. Intrinsically, the excess phonon densities of states of both the large and the small relaxed clusters are practically identical, and this leads to the same kind of excess specific-heat functions in both cases (e.g., same T_{\max} , same decline for increasing T). The only intrinsic differences occur, in $f^c(\omega)$ near $\omega=0$, and in C_v^c near $T=0$ °K. These results invalidate the contention of Genzel and Martin^{2(b)} that relaxation effects might not be important in large crystallites.

A final comment concerns the use of the rigid-ion model. In this model, polarization effects are not taken into account and it is a well-established fact that in most cases the shell model (in one of its various forms), in which polarization is included in a modelistic fashion, is superior to the KRIM in obtaining agreement between theory and experiment. On the other hand, whereas relaxa-

tion calculations in the context of the KRIM are fairly simple, this is by no means the case for the SM. In fact, there are serious difficulties in developing a SM description which is consistent for both static structural properties, such as relaxation, and dynamical properties such as phonon spectra (cf. Ref. 13). Since we are here interested in both kinds of properties, both for small and large clusters, the use of the KRIM is a reasonable point of departure, the more so since up to this time neither relaxed clusters nor large clusters have been treated dynamically.

Finally, since the important differences between the KRIM and the SM are mainly manifested in the optical frequencies, they do not greatly effect the specific heat, which is an integrated quantity determined mainly by the low acoustical frequencies. In fact, in their work on NaCl, Chen *et al.*¹⁶ have found that the KRIM actually leads to better agreement with the experimental results than does the SM. Therefore, for the moment, we consider the use of the KRIM for the evaluation of the low-temperature cluster-excess specific heat as a quite reasonable procedure. Although the present calculations were performed for MgO clusters, the effects of size and of relaxation found here are independent of the actual values of the interaction parameters and it is therefore safe to assume that KRIM calculations for any of the rocksalt structured ionic crystals will lead to the same general conclusions.

*Research supported in part by NSF under Grant Nos. DMR 73-0249-A02 and DMR 75-18492 and by the Robert A. Welch Foundation.

¹R. Ruppin and R. Englman, Rep. Prog. Phys. **33**, 419 (1970).

²(a) L. Genzel and T. P. Martin, Phys. Status Solidi B **51**, 91 (1972); (b) **51**, 101 (1972).

³T. S. Chen and F. W. de Wette, J. Phys. Chem. Solids **37**, 481 (1976).

⁴T. S. Chen, G. P. Alldredge, and F. W. de Wette, Surface Sci. **62**, 675 (1977).

⁵T. S. Chen, G. P. Alldredge, and F. W. de Wette, Phys. Lett. A **46**, 91 (1973).

⁶T. S. Chen, G. P. Alldredge, F. W. de Wette, and R. E. Allen, J. Chem. Phys. **55**, 3121 (1971).

⁷E. W. Kellermann, Philos. Trans. R. Soc. Lond. A **238**, 513 (1940).

⁸P. J. Anderson and A. Scholz, Trans. Farad. Soc. **64**,

2973 (1969).

⁹T. P. Martin, Phys. Rev. B **7**, 3906 (1973).

¹⁰K. H. Rieder and E. M. Hörl, Phys. Rev. Lett. **20**, 209 (1968).

¹¹K. H. Rieder, Surf. Sci. **26**, 637 (1971).

¹²K. H. Rieder (private communication) (cf. Ref. 13).

¹³T. S. Chen, F. W. de Wette, and G. P. Alldredge, Phys. Rev. B **15**, 1167 (1977).

¹⁴W. F. Giauque and R. C. Archibald, J. Am. Chem. Soc. **59**, 561 (1937).

¹⁵T. H. K. Barron, W. T. Berg, and J. A. Morrison, Proc. R. Soc. A **250**, 70 (1959).

¹⁶Confer Refs. 4 and 6; also T. S. Chen, G. P. Alldredge, and F. W. de Wette, in *Proceedings of the Thirteenth International Conference on Low Temperature Physics*, edited by K. D. Timmerhaus, W. J. O'Sullivan, and E. F. Hammel (Plenum, New York, 1974), Vol. 4, p. 441.